RAPID COMMUNICATIONS

PHYSICAL REVIEW E VOLUME 47, NUMBER 4 APRIL 1993

Traveling-wave wall states in rotating Rayleigh-Bénard convection

E. Y. Kuo and M. C. Cross

Condensed Matter Physics 114-36, California Institute of Technology, Pasadena, California 91125

(Received 8 January 1993)

We show that the wall-localized convection states observed in Rayleigh-Bénard convection in rotating cylindrical cells can be explained in terms of a geometry-independent traveling-wave wall state. We calculate the onset Rayleigh number, frequency, and wave number of such a state, as well as its amplitude equation. We also study the large-rotation-rate asymptotic behavior and the small-rotation-rate limit.

PACS number(s): 47.54.+r, 47.20.Bp, 47.32.−y, 47.20.Ky

There have been many studies, both experimental and theoretical, of Rayleigh-Bénard convection in finite rotating systems. Some of the older studies are by Rossby [1], Davies-Jones and Gilman [2], Buell and Catton [3], and Pfotenhauer, Niemela, and Donnelly [4]. In general, heat-transport measurements in the experimental studies found that the onset of convection occurred at Rayleigh numbers *below* that predicted for the infinite unbounded system. This is in contrast to Rayleigh-Bénard convection in a nonrotating system, where the boundaries of the system suppress the onset of convection, and the critical Rayleigh number is greater than that of an infinite system.

Recent experimental studies by Zhong, Ecke, and Steinberg [5] and Ning and Ecke [6] employing the shadowgraph visualization technique have shown that the convection states that occur below the infinite-system critical Rayleigh number exist along the sidewalls of the rotating cell, and precess counter to the direction of rotation. Furthermore, the theoretical study of convection in rotating cylinders by Goldstein *et al.* [7], in which they solved for the fluid equations in the full cylindrical geometry, found the existence of precessing modes localized near the sidewalls of the cylinder at Rayleigh numbers below the infinite-system critical Rayleigh number.

In this paper we show that these states are not just a feature of small-aspect-ratio systems as might be thought from the earlier studies [2,3], instead we show that they can be explained in terms of a traveling-wave wall state, the existence of which depends only upon the presence of the sidewall, and the addition of the Coriolis force in the equations of motion of the fluid. The onset below that for the unbounded system will therefore persist even for large-aspect-ratio systems. This system thus provides an example of the existence of wall-localized states induced by boundary conditions in pattern-forming systems previously suggested by Kramer and Hohenberg [8] from general arguments. Idealizing the sidewall state as a geometry-independent state allows for much simplification in calculating the characteristics of the observed convection states, just as does the concept of the unbounded infinite system for the familiar bulk roll state. In this approach, the sidewall state is essentially one dimensional in nature, characterized by its wave number along the wall and its frequency. The characteristics of a convection state in a real physical geometry may be calculated in terms of finite-size corrections to these asymptotic results.

We are able, with relative ease, to calculate the characteristics of this wall state in the idealized case of an infinite, straight sidewall, for free-slip top and bottom boundary conditions. The calculations should be readily generalizable to no-slip top and bottom boundary conditions. The effect of realistic sidewall boundary conditions—including the thickness, and thermal conductivity and diffusivity of the wall—are easily incorporated into the calculation. We can also study the asymptotic behavior at large rotation rates, as well as the small-rotation-rate region, where the wall state connects to the bulk state. Moreover, since the wall state is quasi-one-dimensional, its dynamics can be described by a one-dimensional complex amplitude equation, and we calculate its parameters to lowest nonlinear order. We find that (for free-slip top and bottom boundary conditions) the bifurcation is forward; thus, rotating Rayleigh-Bénard convection in large-aspect-ratio systems may provide a convenient experimental realization of a traveling-wave instability with a forward bifurcation, and is therefore worthy of further theoretical and experimental study.

We consider convection in a rotating semi-infinite horizontal layer of fluid with one straight infinite sidewall. The angular velocity $\mathbf{\Omega}_D=\Omega_D\hat{\mathbf{z}}$ is constant and in the vertical direction.

We use the usual dimensionless variables in which length is measured in units of the cell height d, time in units of the thermal diffusion time d^2/κ (κ is the thermal diffusivity of the fluid), and temperature in units of $\kappa\nu/\alpha g d^3$ (ν is the kinematic viscosity, α the coefficient of thermal expansion, and g the gravitational acceleration). In these units, the equations of motion for the fluid velocity $\mathbf{v}=(u,v,w)$, the deviation of the pressure from its linear conduction profile, θ, the deviation of the pressure from its conduction profile, p, and the incompressibility condition, are

$$\sigma^{-1}[\partial\mathbf{v}/\partial t+(\mathbf{v}\cdot\nabla)\mathbf{v}]=-\sigma^{-1}\nabla(p/\rho_0)+\theta\hat{\mathbf{z}}+2\Omega\mathbf{v}\times\hat{\mathbf{z}}+\nabla^2\mathbf{v}\,, \tag{1}$$

$$\partial\theta/\partial t+(\mathbf{v}\cdot\nabla)\theta=Rw+\nabla^2\theta\,, \tag{2}$$

$$\nabla\cdot\mathbf{v}=0\,. \tag{3}$$

Here $\Omega=\Omega_D d^2/\nu$ is the dimensionless angular velocity, $R=\alpha g(\Delta T)d^3/\kappa\nu$ is the Rayleigh number (ΔT is the tem-

perature difference between the bottom and top plates), $\sigma=\nu/\kappa$ is the Prandtl number, while ρ_0 is the mean fluid density. The term due to the centrifugal force, $-(\theta\sigma^2/2\tilde{g})\nabla|\Omega\times\mathbf{r}|^2$, which would be on the right-hand side of (1), has been neglected ($\tilde{g}$ is the gravitational acceleration in the units above). In practice, this term is negligible compared to the gravitational buoyancy term if $\Omega_D^2 l/g \ll 1$, where l is the radius of the cell.

We will take the coordinate system to be such that the height of the cell is from $z=0$ to $z=1$, and the sidewall runs along the x axis at $y=0$, with the fluid occupying the positive y half of the xy plane. The sidewall lies in the negative y half of the plane, and is of arbitrary thickness. With this setup, the boundary conditions at the bottom, $z=0$, and the top, $z=1$, are the (unphysical) free-slip fluid boundary conditions and the physical thermal boundary condition

$$w=\partial u/\partial z=\partial v/\partial z=0\ ,\quad \theta=0\ , \tag{4}$$

and those at the sidewall, $y=0$, are the physical no-slip fluid boundary conditions and the continuity of heat

$$u=v=w=0\ ,\quad \partial\theta/\partial y-\mu\theta=0\ , \tag{5}$$

where μ depends not only on the thermal properties of the sidewall and the fluid, but also upon the nature of the solution in the fluid.

The unphysical free-slip boundary conditions have often been used in convection problems to allow a simple calculation that may illustrate the behavior of the more physical no-slip boundary conditions. In this particular case, there are reasons to believe the calculation may be quite accurate, and even exact for the linear terms in the large-rotation-rate limit. In their paper [7], Goldstein *et al.* showed that in finite cylindrical cells, at least for large rotation rates, the critical Rayleigh number, precession frequency, and azimuthal mode number of the "fast mode," which corresponds to the traveling-wave wall state, do not depend strongly upon whether one uses the free-slip or the no-slip boundary conditions at the top and bottom plates. Also, Clune and Knobloch [9] showed that for the bulk state, the no-slip and free-slip solutions to the linear stability problem become identical as $\Omega\to\infty$. Similar arguments justify our use of the free-slip boundary conditions for the purposes of calculational simplicity. The reason for this weak difference between free-slip and no-slip boundary conditions, particularly at large rotation rates, is the existence of thin $[\sim(\nu/\Omega_D)^{1/2}]$ Ekman boundary layers in the case of no-slip boundary conditions. Outside the thin boundary layers, the dominant mode may be similar to the mode for free-slip boundary conditions, and thus the linear onset solution will have similar critical parameters. This, however, probably does not hold for nonlinear calculations, which involves coupling the dominant mode to other modes.

Traveling-wave wall states should have a basic space and time dependence that $\sim\exp[i(q_x x-\omega t)]$. Thus to find the lowest Rayleigh number critical onset wall state, we seek solutions of Eqs. (1)–(3) of the form (the components of χ are the physical variables we are interested in)

$$\chi(x,y,z,t)=\chi_0(y,z)e^{i(q_x x-\omega t)}+\text{c.c.}$$

for different q_x, which also satisfy the boundary conditions (4) and (5), as well as the condition that χ not diverge as $y\to+\infty$. The solution with the lowest onset Rayleigh number is then the critical onset wall state, and we have thus found R_c, ω_c, and q_{xc}, the critical Rayleigh number, precession frequency, and wave number of the traveling-wave wall state.

Equations (1)–(3) can be linearized and combined to give a dispersion relation that is fourth order in $q_x^2+q_y^2$. Thus for free-slip top and bottom boundary conditions, we can write for the onset state

$$\chi_0(y,z)=\begin{bmatrix}u_0(y,z)\\ v_0(y,z)\\ w_0(y,z)\\ \theta_0(y,z)\end{bmatrix}=\sum_{j=1}^{4}e^{iq_{yj}y}\begin{bmatrix}U_{0j}\cos\pi z\\ V_{0j}\cos\pi z\\ W_{0j}\sin\pi z\\ \Theta_{0j}\sin\pi z\end{bmatrix},$$

where q_y is complex, as are U_0, V_0, W_0 and Θ_0, and of each pair of q_y's satisfying the dispersion relation with equal value of q_y^2, only the one that allows $\chi\to0$ when $y\to+\infty$ is included. The boundary conditions at the top and bottom (4) are thus automatically satisfied. For a solution of this form, the value of μ in (5) is

$$\mu=K_w k_w\tanh(k_w l_w)\ , \tag{6}$$

where K_w is the ratio of the thermal conductivity of the sidewall to that of the fluid, l_w is the width of the sidewall, and with κ_w the thermal diffusivity of the sidewall,

$$k_w^2=(q_x^2+\pi^2-i\kappa_w^{-1}\omega)\ . \tag{7}$$

To satisfy the sidewall boundary conditions (5) we first use the (linearized) equations of motion (1)–(3) to solve for U_{0j}, V_{0j}, and W_{0j} in terms of Θ_{0j}. The four sidewall boundary conditions then become a 4×4 *complex* matrix condition on $\Theta_0=(\Theta_{01},\Theta_{02},\Theta_{03},\Theta_{04})$. For given q_x we can find, numerically, R and ω, such that the characteristic equation of this complex matrix condition is satisfied, and then find the eigenvectors of the matrix to give the form of the onset solution.

This gives the onset Rayleigh number and frequency for a *given* q_x. Minimizing the onset Rayleigh number with respect to q_x, we find the critical Rayleigh number R_c, the critical frequency ω_c, and the critical wave number q_{xc}. Figure 1 shows R_c, ω_c, and q_{xc}, respectively, as a function of the rotation rate for Prandtl number σ equal to 6.4 and thermal boundary conditions $K_w=0.25$, $\kappa_w=1$, and $l_w=0.15$. (Note that the values of ω_c are actually negative.) This corresponds to the experimental conditions of Ref. [6].

Near onset, the traveling-wave wall state may experience slow modulations in both space and time (along the wall), and the dynamics may be calculated by expanding in a small parameter $\epsilon=(R-R_c)/R_c$. The amplitude A is the complex envelope of the basic traveling wave, $\exp[i(q_{xc}-\omega_c t)]$, i.e., the physical quantities are

$$\chi(x,y,z,t)=A(x,t)e^{i(q_{xc}x-\omega_c t)}\chi_0(y,z)+\text{c.c.}+\text{h.o.t.}\ ,$$

where $A\sim\epsilon^{1/2}$ and the higher-order terms (h.o.t.) are $O(\epsilon)$. The amplitude equation is one dimensional in the sense that the dynamics of the amplitude depend only upon the spatial variations parallel to the sidewall, and can be written

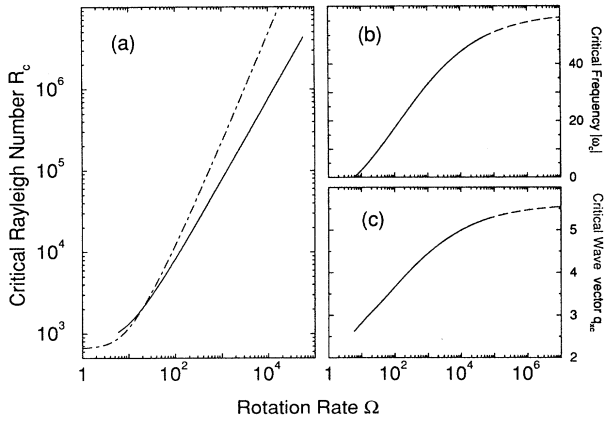

FIG. 1. Critical onset parameters for the wall state for the experimental conditions of Ref. [6] vs the dimensionless rotation rate Ω. (a) Critical Rayleigh number R_c: (solid line) wall state; (dash-dotted line) bulk mode. (b) Magnitude of the critical frequency ω_c: (solid line) numerical work; (dashed line) asymptotic calculation. (c) Critical wave vector q_{xc}: (solid line) numerical work; (dashed line) asymptotic calculation.

$$\tau_0\left[\frac{\partial A}{\partial t}+s\frac{\partial A}{\partial x}\right]=\epsilon(1+ic_0)A+\xi_0^2(1+ic_1)\frac{\partial^2 A}{\partial x^2}-g(1+ic_3)|A|^2A \tag{8}$$

to lowest nonlinear order. The parameters s, τ_0, ξ_0, g, c_0, c_1, and c_3 are (real-valued) parameters that can be calculated and measured. s is easily seen to be the group velocity, and τ_0 and ξ_0 are the time and length scales of the modulation respectively. The cubic term turns out to have negative real part (g is positive); thus the solution A saturates when $|A|\sim\epsilon^{1/2}$, and the bifurcation is forward.

The parameters in the linear part of the amplitude equation can be calculated by finding (numerically) the complex growth rate $\Gamma=\gamma-i(\omega_c+\Delta\omega)$ as a function of $\epsilon=(R-R_c)/R_c$ and the wave-number difference $k=q_x-q_{xc}$ for small ϵ and small k, such that, as in calculating the onset parameters, the dispersion relation and boundary conditions are satisfied for the solution found for the linearized equations of motion. [Here the value of μ in the thermal boundary condition is calculated in (6) by changing $-i\omega$ in (7) to $\Gamma=\gamma-i\omega$.]

We have also developed the expansion in the nonlinearity to third order to calculate the real and imaginary parts of the coefficient of the nonlinear term in the amplitude equation. The method, which is standard [10], will be described in detail elsewhere. We point out here, however, that since the linear solution is a sum of exponentials, the whole procedure may be carried out analytically, except for the numerical solution of the dispersion relation to find the wave vectors of the linear solution and of the second-order, nonlinear homogeneous solution. The constant g depends on a choice of normalization: we normalize such that the ratio of the convected heat to the heat conducted through a strip of fluid of width equal to the cell height is $|A|^2$.

The various parameters of the amplitude equation are shown in Fig. 2 as a function of the rotation rate, again for Prandtl number σ equal to 6.4 and thermal boundary conditions as before. It is worth pointing out that the group velocity s, which is positive, is in the opposite direction to the phase velocity ω_c/q_c, which is negative. We also note that, at least for our calculations, there is no Benjamin-Feir instability, as $1+c_1c_3>0$.

In Fig. 1(a) the critical onset Rayleigh numbers of both the traveling-wave wall state and the stationary bulk convection state that occurs in infinite unbounded systems are plotted as a function of the rotation rate. In contrast to the "large"-rotation-rate region where the traveling-wave wall state has the lower onset, below a critical rotation rate Ω_c, the bulk state has the lower onset, and would be the convection state that actually occurs first as the Rayleigh number is increased. As can be seen from Fig. 1(a), however, the wall state persists below Ω_c, but not all the way to zero rotation rate. Instead, we find that the frequency goes linearly to zero at a nonzero rotation rate, as shown in Fig. 1(b). (Although we are plotting the values of R_c and ω_c for the critical wave vectors, which vary as a function of Ω, these conclusions remain true if instead we use a fixed wave vector q_x.) At this same rotation rate the spatial decay rate $\mathrm{Im}\,q_y$ also goes to zero, while $\mathrm{Re}\,q_y$ goes to a nonzero constant. Thus, rather surprisingly, we find that the wall mode bifurcates continuously from a bulk mode at a particular orientation to the sidewall (given by $\mathrm{Re}\,q_y/q_x$). The nature of this bifurcation is explored further in Fig. 3, where we show the critical Rayleigh number plotted against the wave vector parallel to the wall for the wall mode (solid line) and the bulk mode that connects to the wall mode (dash-dotted line) for a particular rotation rate. For this rotation rate the wall mode has the lower minimum Rayleigh number, and would be the first mode to go unstable if the wave vector q_x were free to adjust. For large q_x, however, the wall mode disappears at the codimension-2 point P. The inset shows how the frequency and the spatial decay rate of the wall mode go to zero as q_x varies.

The application of these results to a finite experimental system is quite delicate. In a finite system the bulk modes

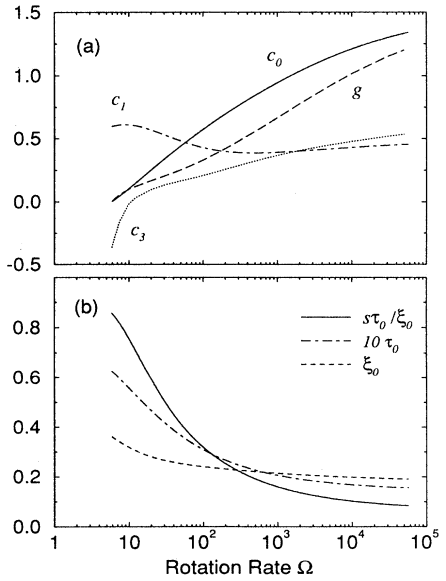

FIG. 2. Amplitude equation parameters defined by Eq. (8) for the wall state for the experimental conditions of Ref. [6] vs Ω.

would be expected to gain a small rotation rate (probably going as L^{-1}, where L is the size of the system). Thus we would expect to see either a bifurcation or a rapid crossover between two finite frequency modes, with one having a frequency largely independent of aspect ratio (the wall mode) and the other having a frequency becoming smaller as the aspect ratio is increased (the bulk mode). The structure of the bifurcation as shown in Fig. 3 may also have implications for the transition between the two states in the nonlinear regime as the Rayleigh number is increased.

In the case of the bulk convection state in an infinite unbounded system, Chandrasekhar [11] showed that, when the rotation rate is large, the asymptotic behavior of R_c and q_c for both free-slip and no-slip top and bottom boundary conditions is $R_c \sim \Omega^{4/3}$ and $q_c \sim \Omega^{1/3}$.

We find that the traveling-wave wall state has a different asymptotic limit at large rotation rates, and that this limit also depends upon the thermal boundary condition imposed at the sidewall. In the case of insulating, or nonperfectly conducting sidewalls, we find the asymptotic behavior to be $R_c \sim \Omega$, $q_{xc} \rightarrow$const, and $\omega_c \rightarrow$const in the limit $\Omega \rightarrow \infty$. In the case of perfectly conducting sidewalls, the asymptotic behavior appears more complicated, but numerics and a balance of terms in the dispersion relation would indicate that it is $R_c \sim \Omega^{4/3}$, $q_{xc} \sim \Omega^{1/6}$, and $\omega_c \sim \Omega^{1/3}$, as $\Omega \rightarrow \infty$.

In the former case we have solved for the exact asymptotic solution at large Ω. We find the onset Rayleigh number and frequency at wave vector q_x to be given by the solution of

$$(\pi + iq_x)(iq_y - \mu) + \bar{R} q_x = 0 , \tag{9}$$

with $\mu(q_x,\omega)$ given by (6) and $\bar{R} = R/2\pi\Omega$, and where $q_y = (-i\omega - q_x^2 - \pi^2)^{1/2}$ is the complex wave-vector component giving the decay perpendicular to the wall. For the parameters and boundary conditions quoted earlier, this yields $R_c \rightarrow 74.40\Omega$, $\omega_c \rightarrow -57.68$, $q_{xc} \rightarrow 5.545$. For the insulating case $\mu = 0$, (9) can be solved analytically for $R(q_x)$ and $\omega(q_x)$. In this case we find $R_c \rightarrow 63.64\Omega$, $\omega_c \rightarrow -66.05$, $q_{xc} \rightarrow 6.069$. Fits to our numerical results up to $\Omega = 50\,000$, assuming corrections to the asymptotic limit go as a polynomial in $\Omega^{-1/3}$ give good agreement with these values. [See the dashed lines in Figs. 1(b) and 1(c)].

The asymptotic behavior for the special case of perfectly conducting boundaries is more involved, and we do not have analytic results here.

In conclusion we have proposed considering the new state in rotating convection that preempts the bulk onset for large rotation rates as a one-dimensional wave with an onset enhanced by the presence of a sidewall in a semi-infinite system. This simplifies the calculation of many properties of the linear onset solution and the nonlinear state. We have illustrated this using the model of free-slip upper and lower boundaries, and have presented several novel results, including the large- and small-rotation-rate limits of the onset, and all the coefficients of the amplitude equation describing the nonlinear state. Many of these results will be accurate for the physical case of no-slip boundaries for large rotation rates.

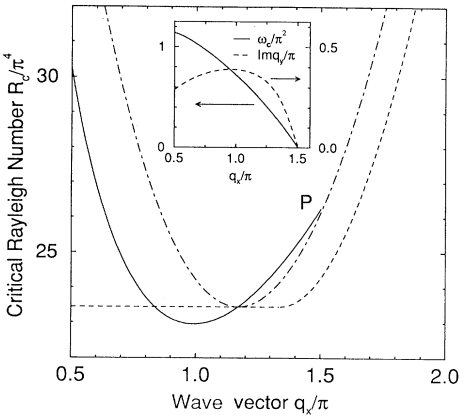

FIG. 3. Critical Rayleigh number R_c vs q_x for a fixed rotation rate $\Omega = 4.5$ for the experimental conditions of Ref. [6]. The wall mode (solid line) merges with a bulk mode (dash-dotted line) at the codimension-2 point P. Note that this dash-dotted line is drawn for the particular q_y of the bulk mode from which the wall mode bifurcates at P. The dashed line shows the *lowest* bulk Rayleigh number, allowing q_y to vary. The inset shows the critical frequencies ω_c (solid) and the inverse decay lengths $\mathrm{Im}\, q_y$ (dashed) of the wall mode; both ω_c and $\mathrm{Im}\, q_y$ go to zero at P.

Note added in proof. We recently became aware of work by J. Herrmann and F. H. Busse [J. Fluid Mech. (to be published)] that independently arrives at similar results for R_c, ω_c, and q_{xc} for the cases of perfectly conducting and insulating sidewalls. In addition, they present new analytic results for the large frequency asymptotic values for the conducting sidewalls: the suggestions we made in this case based on numerical results are consistent with these analytic expressions. We have also found out (private communication) that M. L. van Hecke and W. van Saarloos have performed similar calculations to ours in a slab geometry.

We wish to thank L. Ning and R. E. Ecke for sharing their experimental results with us prior to publication, and Y. Tu for useful discussions. This work was supported with funds from the NSF through Grant No. DMR-9013984.

[1] H. T. Rossby, J. Fluid Mech. **36**, 309 (1969).
[2] R. P. Davies-Jones and P. A. Gilman, J. Fluid Mech. **46**, 65 (1971).
[3] J. C. Buell and I. Catton, Phys. Fluids **26**, 892 (1983).
[4] J. M. Pfotenhauer, J. J. Niemela, and R. J. Donnelly, J. Fluid Mech. **175**, 85 (1987).
[5] F. Zhong, R. E. Ecke, and V. Steinberg, Phys. Rev. Lett. **67**, 2473 (1991).
[6] L. Ning and R. E. Ecke (unpublished).
[7] H. F. Goldstein *et al.*, J. Fluid Mech. **248**, 583 (1993).
[8] L. Kramer and P. C. Hohenberg, Physica **13D**, 357 (1984).
[9] T. Clune and E. Knobloch, Phys. Rev. A **47**, 2536 (1993).
[10] A. C. Newell and J. A. Whitehead, J. Fluid Mech. **38**, 279 (1969).
[11] S. Chandrasekhar, *Hydrodynamic and Hydromagnetic Stability* (Oxford University Press, Oxford, 1961).